(Ga,Mn)As based superlattices and the search for antiferromagnetic interlayer coupling

A. D. Giddings,[1] T. Jungwirth,[1,2] and B. L. Gallagher[1]
[1]*School of Physics and Astronomy, University of Nottingham, Nottingham NG7 2RD, United Kingdom*
[2]*Institute of Physics ASCR, v.v.i., Cukrovarnická 10, 162 53 Praha 6, Czech Republic*
(Received 2 February 2008; revised manuscript received 8 July 2008; published 10 October 2008)

Antiferromagnetic interlayer coupling in dilute magnetic semiconductor superlattices could result in the realization of large magnetoresistance effects analogous to the giant magnetoresistance seen in metallic multilayer structures. In this paper we use a mean-field theory of carrier induced ferromagnetism to explore the multidimensional parameter space available in (Ga,Mn)As based superlattice systems. Based on these investigations we examine the feasibility of creating a superlattice that exhibits antiferromagnetic coupling and suggest potentially viable recipes.

DOI: 10.1103/PhysRevB.78.165312 PACS number(s): 73.61.Ey, 75.50.Pp, 75.70.Cn

I. INTRODUCTION

The exciting prospect of spin based electronics, known as spintronics, was initiated in 1988 with the discovery of giant magnetoresistance (GMR) in metallic multilayer structures.[1–3] These structures consist of interposed ferromagnetic (FM) and non-FM layers. When the magnetization of adjacent FM layers is aligned in antiparallel directions, enhanced spin scattering of carriers causes an increased electrical resistance through the layers, while when they are parallel the resistance is lower. Although typical GMR devices today consist of a trilayer structure with a pinned magnetic layer and one in which the magnetization is free to rotate, another method of implementation is with a superlattice structure where adjacent layers have an antiparallel magnetization unless an external field is applied to align them.

In multilayer structures containing ferromagnetic layers, in addition to the ferromagnetic order within the layers, there can also exist magnetic exchange between the layers. The mechanism that causes the magnetic order between the layers is known as interlayer exchange coupling (IEC) and has been shown in metallic systems to be due to the spin polarization of conduction carriers.[4]

Because the IEC energy considers the spin dependent changes in total energy, it thus determines which magnetic alignment of adjacent layers is energetically favorable. Although complicated helical arrangements can exist,[5] typically the interlayer exchange coupling will either be FM, where there is a parallel alignment of magnetization, or antiferromagnetic (AFM) where there is an antiparallel alignment. Therefore, in such a system, achieving AFM interlayer coupling is of high importance for technological applications.

In addition to existing in metal systems, IEC is a generic property of magnetic multilayers, and AFM IEC has even been demonstrated in nonmetallic FM semiconductor systems based on all-semiconductor EuS/PbS superlattices.[6] AFM IEC in dilute magnetic semiconductor (DMS) based superlattices was theoretically predicted in 1999 using a $\mathbf{k}\cdot\mathbf{p}$ kinetic-exchange model for carrier mediated ferromagnetism.[7] This approach considers delocalized charge and adds extra modulation induced by spin-polarized effects. A large magnetoresistance (MR) was predicted due to the large difference in miniband dispersion for the cases of ferromagnetically and antiferromagnetically aligned layers. Recently, IEC has been further explored using a tight-binding model.[8] This complementary microscopic approach, although not self-consistent, takes into account atomic orbitals for all the constituent atoms, leading to more accurate descriptions of the band structure. Despite the different approaches used, both methods provide qualitatively similar results for the IEC, which shows oscillatory Ruderman-Kittel-Kasuya-Yosida (RKKY)-like behavior.

Although IEC has been shown to exist in DMS systems based on (Ga,Mn)As/(Al,Ga)As trilayers,[9] there have been no reports of AFM interlayer coupling. Experimental work into (Ga,Mn)As based multilayer and superlattice structures has only succeeded in demonstrating FM IEC.[10,11] In order to test the prediction of a phenomenon analogous to GMR in metals in DMS materials with a potentially much greater MR ratio, it is essential that AFM interlayer coupling is obtained.

The aim of this study is to provide a comprehensive description of the multidimensional parameter space available in these DMS superlattice systems in order to identify optimal parameters for realizing an antiferromagnetically coupled system. Because the interlayer coupling is mediated by carriers, a $\mathbf{k}\cdot\mathbf{p}$ approach is more practical for exploring a wide range of parameter values. The limitation of this approach is that a single parabolic band approximation is used, sacrificing full quantitative accuracy for qualitative descriptions of a wide range of systems. Subtleties of the band-structure and spin-orbit effects are neglected. However, qualitative agreement with the data published in Ref. 8 at least partially justifies this approach.

The organization of this paper is as follows: first the details of the theoretical modeling of a DMS based superlattice system and the numerics of the self-consistent mean-field calculations will be shown. Next, the results, which will primarily consider (Ga,Mn)As based superlattice systems with either GaAs or (Al,Ga)As nonmagnetic spacer layers, will be presented. Finally, in Sec. IV, suggestions for recipes for superlattice systems in which antiferromagnetic interlayer coupling may occur will be given.

II. THEORETICAL MODELING

Our calculations are based on the Zener kinetic-exchange model[12] description of magnetic interactions in Mn-doped

III–V semiconductor structures. Microscopically, the kinetic exchange between the local Mn moments and itinerant hole spins originates from the *p-d* orbital hybridization.[13] This model provides a good description of ferromagnetism in bulk (Ga,Mn)As when the detailed structure of the valence band is taken into account.

An intuitive picture of the IEC in (III,Mn)V/III–V multilayer structures can be obtained by the perturbative mapping of the kinetic-exchange model onto an effective interaction between local moments following the RKKY approach.[7] The RKKY theory can be expected to provide useful predictions for structures close to a model pseudo-one-dimensional (1D) system consisting of alternating thin ferromagnetic layers and nonmagnetic spacer layers such that there is small coupling and low carrier polarization.[14] The RKKY range function falls off asymptotically with $\frac{\sin(2k_F d)}{d^2}$, where k_F is the carrier wave vector and d is the distance between the magnetic layers. Thus, the RKKY theory shows that the coupling can have an oscillatory form.

The Zener kinetic-exchange model for homogeneous (Ga,Mn)As was generalized in Ref. 7 in order to account for the RKKY-like oscillatory effects in the inter-(Ga,Mn)As coupling in (Ga,Mn)As-based ferromagnetic/nonmagnetic superlattices on a more quantitative level. In this model the band structure is solved using the kinetic-exchange model and a parabolic band $\mathbf{k}\cdot\mathbf{p}$ effective-mass approximation. In the Hamiltonian the magnetic moments are accounted for through the *p-d* kinetic-exchange interaction between Mn spins and hole spins which is parametrized by a constant J_{pd} and treated in the mean-field virtual crystal approximation. The value of J_{pd} can be experimentally determined, and modern estimates of this value place it at 55 meV nm^3.[15] To account for the inhomogeneity, a standard formalization of the local spin-density approximation (LSDA) using the Kohn-Sham equations for inhomogeneous systems is used in the band-structure calculations.[16] Hole mass is $m^*=0.5m_e$ and the spin of local Mn moments is $S=\frac{5}{2}$ at $T=0$ K. Thermodynamics are treated on a mean-field level.

In order to find the normalized wave function for a given energy, Bloch's theorem is used to solve the one-dimensional time-independent spin-dependent Schrödinger equation,

$$\left(\frac{p^2}{2m^*}+V_\sigma(z)\right)\Psi_{k,n,\sigma}(z)=E_{k,n,\sigma}\Psi_{k,n,\sigma}(z), \tag{1}$$

which we shall rewrite as

$$\frac{d^2\Psi_{k,n,\sigma}}{dz^2}=\frac{2m^*}{\hbar^2}[V_\sigma(z)-E_{k,n,\sigma}]\Psi_{k,n,\sigma}(z),$$

$$\Psi''(z)=f\Psi(z), \tag{2}$$

where k is the wave vector, n is the subband index, σ is the spin index, and $f=\frac{2m^*}{\hbar^2}[V_\sigma(z)-E]$.

The Bloch function,

$$\Psi_{k,n,\sigma}(z)=u_{k,n,\sigma}(z)e^{(ikz)}, \tag{3}$$

gives the solutions of the Schrödinger equation for a periodic potential.

For this system, the explicit form of the Hamiltonian for the spin-dependent potential $V_\sigma(z)$ is given by

$$V_\sigma(z)=V_H+V_{xc,\sigma}+V_b-\frac{\sigma}{2}[g^*\mu_B B+h_{pd}(z)], \tag{4}$$

where V_H is the Hartree (electrostatic) potential given by the Poisson equation, $V_{xc,\sigma}$ is the spin-dependent exchange-correlation potential given by the LSDA equation, V_b is the band offset, g^* is the free-carrier g-factor, and h_{pd} is the mean-field kinetic-exchange interaction.[7] The IEC energy, E_c, is defined as the difference in energy between the FM and AFM states per superlattice period.

Let us suppose that our one-dimensional lattice has a period d_{n+m} and consider now the solution only at N evenly distributed discrete points on the z axis with a separation h. The wave function at each point is denoted as $\Psi(z)$. By Taylor's theorem, the second-order approximations for $\Psi(z+h)$ and $\Psi(z-h)$ are

$$\Psi(z+h)=\Psi(z)+h\Psi'(z)+\frac{h^2}{2}\Psi''(z), \tag{5}$$

$$\Psi(z-h)=\Psi(z)-h\Psi'(z)+\frac{h^2}{2}\Psi''(z). \tag{6}$$

Taking the sum of Eqs. (5) and (6) we obtain

$$h^2\Psi''(z)=\Psi(z+h)+\Psi(z-h)-2\Psi(z). \tag{7}$$

Substituting the Schrödinger equation from Eq. (2) into Eq. (7) and rearranging gives the wave function at a given point as a linear combination of the wave functions at the two previous points;

$$\Psi(z+h)=(h^2f+2)\Psi(z)-\Psi(z-h). \tag{8}$$

This linear transformation can be represented as a transfer matrix, $\mathbf{M}_n$, such that

$$\mathbf{M}_n\begin{pmatrix}\Psi_n\\ \Psi_{n-1}\end{pmatrix}=\begin{pmatrix}m_{n,11} & m_{n,12}\\ m_{n,21} & m_{n,22}\end{pmatrix}\begin{pmatrix}\Psi_n\\ \Psi_{n-1}\end{pmatrix}=\begin{pmatrix}\Psi_{n+1}\\ \Psi_n\end{pmatrix}, \tag{9}$$

where Ψ_n is the wave function at the nth z point. By inspection we see that $m_{n,11}=h^2f+2$, $m_{n,12}=-1$, $m_{n,21}=1$, and $m_{n,22}=0$. It is worth noting here that the determinant of each $\mathbf{M}_n$, $\det(\mathbf{M}_n)=1$. The product of the N transfer matrices $\Pi_{n=1}^{N}\mathbf{M}_n=\mathbf{M}^T$ represents the transformation from Ψ_0 to Ψ_N. By Bloch theorem's periodic boundary condition, Eq. (3), this transformation can be written as

$$\mathbf{M}^T\begin{pmatrix}\Psi_1\\ \Psi_0\end{pmatrix}=\begin{pmatrix}m_{11}^T & m_{12}^T\\ m_{21}^T & m_{22}^T\end{pmatrix}\begin{pmatrix}\Psi_1\\ \Psi_0\end{pmatrix}=\begin{pmatrix}\Psi_{N+1}\\ \Psi_N\end{pmatrix}=e^{ika}\begin{pmatrix}\Psi_1\\ \Psi_0\end{pmatrix}. \tag{10}$$

Therefore,

$$\begin{aligned}0&=\det(\mathbf{M}^T-e^{ika}\mathbf{I}_2)=(m_{11}^T-e^{ika})(m_{22}^T-e^{ika})-m_{12}^Tm_{21}^T\\&=m_{11}^Tm_{22}^T-m_{12}^Tm_{21}^T-e^{ika}(m_{11}^T+m_{22}^T)+e^{2ika}\\&=\det(\mathbf{M}^T)-e^{ika}\,\mathrm{Tr}(\mathbf{M}^T)+e^{2ika}.\end{aligned} \tag{11}$$

Since the determinant of $\mathbf{M}_n$ is 1, then the determinant of any product of $\mathbf{M}_n$, for any n, will also have a determinant of

1, hence $\det(\mathbf{M}^T)=1$. Substituting this into Eq. (11) gives

$$1 - e^{ika}\,\mathrm{Tr}(\mathbf{M}^T) + e^{2ika} = 0, \tag{12}$$

$$\mathrm{Tr}(\mathbf{M}^T) = e^{ika} + e^{-ika} = 2\cos(ka). \tag{13}$$

For a given energy, wave vector k can thus be found by

$$k = \frac{1}{a}\arccos\left(\frac{1}{2}\mathrm{Tr}(\mathbf{M}^T)\right), \tag{14}$$

and the corresponding wave function can be found similarly.

III. RESULTS

In the RKKY model of interlayer exchange the oscillations occur as a function of $k_F d$, where k_F is the Fermi wave vector and d is the separation between the two-dimensional (2D) magnetic planes.[17] In our model we shall denote d_n as the width of the nonmagnetic layers, corresponding to d from the RKKY model, and d_m as the width of the magnetic layers. The length of a GaAs unit cell is labeled a_0 and has a value of 0.565 nm. We shall also define the average Fermi wave vector $\bar{k}_F$ as

$$\bar{k}_F = (3\pi^2 \bar{N}_{3D})^{1/3}, \tag{15}$$

corresponding to the Fermi vector k_F in the ideal RKKY model with a parabolic band. The average three-dimensional (3D) carrier concentration $\bar{N}_{3D}$ is defined as

$$\bar{N}_{3D} = \frac{1}{d_{n+m}}\int_{\text{unit cell}} N_{3D}(z)dz = \frac{N_{2D}}{d_{n+m}}. \tag{16}$$

The superlattice structures being considered in this paper consist of thin (Ga,Mn)As layers interposed with nonmagnetic spacer layers. The primary structural parameters that can be changed are the widths of the layers and their composition. Figure 1(a) shows the calculated self-consistent charge distribution and potentials for a simple case with a low moment concentration (2%), and the spacer layers are thicker than the magnetic layers. There is a uniform impurity concentration of acceptors throughout the structure, either magnetic, like Mn in the magnetic layers, or from nonmagnetic dopants in the spacer layers. The polarization of carriers is low in this case, and they have an almost totally uniform distribution. These figures show cases where the number of monolayers of nonmagnetic layer $d_n/\frac{1}{2}a_0=5$ and average 3D carrier concentration $\bar{N}_{3D}=10^{20}$ cm^{-3}. The Fermi energy is at $V_\sigma=0$ eV. The interlayer coupling is in an assumed AFM state, although this may not be the energetically favored state for such a system.

The effect of increasing the number of moments in the magnetic layers is shown in Fig. 1(b) where the Mn doping is 8%. As expected, the increased moment concentration increases the size of spin splitting in the magnetic layers, which increases the carrier polarization. Additionally, the potential due to the magnetic ordering causes a redistribution of carriers to occur, increasing the concentration in the magnetic layer. Another way to cause carrier redistribution is to remove the doping from the nonmagnetic layer, which is shown in Fig. 1(c), where the Mn concentration in the magnetic layers is again 2%. Without a neutralizing background charge, Coulomb repulsion opposes carrier redistribution into the nonmagnetic layers. The resulting carrier distribution is similar to that of Fig. 1(b). Although there is a greater concentration of carriers in the magnetic layers, the polarization is not significantly increased over that seen in Fig. 1(a) where there is a uniform charge concentration.

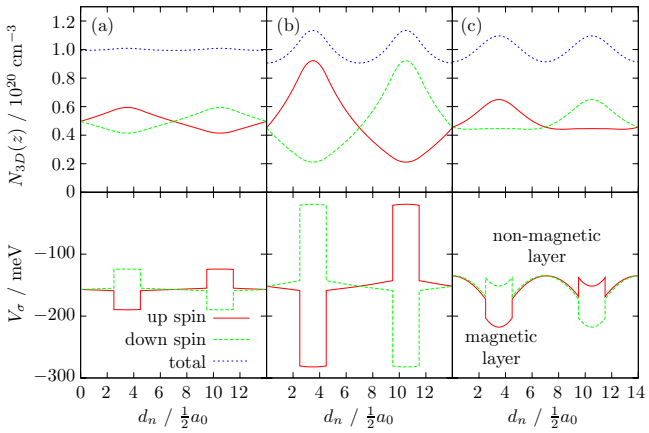

FIG. 1. (Color online) The self-consistent charge distribution, N_{3D}, and potentials, V_σ, for a double unit cell of three different (Ga,Mn)As/GaAs based superlattice structures in an AFM state. $d_m/\frac{1}{2}a_0=2$, $d_n/\frac{1}{2}a_0=5$, and $\bar{N}_{3D}=10^{20}$ cm^{-3} in each case. $V_\sigma=0$ eV corresponds to the Fermi level. (a) 2% Mn doping and a uniform impurity concentration, (b) 8% Mn doping and a uniform impurity concentration, and (c) 2% Mn doping but no impurities in the nonmagnetic layer.

To cause stronger confinement of carriers to the magnetic layers, the nonmagnetic layers can be made from (Al,Ga)As. The effects of this are shown in Fig. 2(a), where the carrier concentration in the center of the magnetic layers is about double that of the center of the nonmagnetic layers. Although

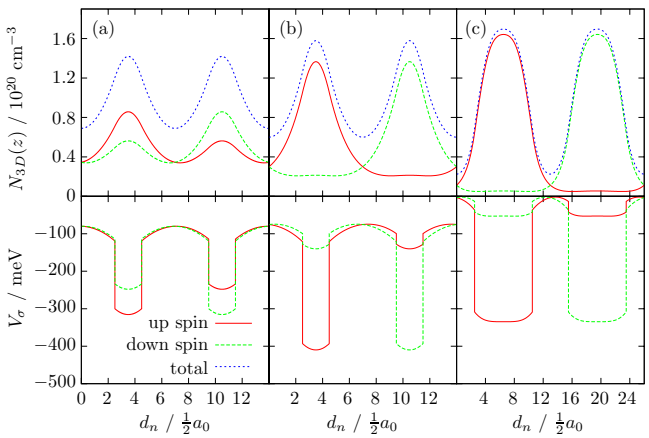

FIG. 2. (Color online) The self-consistent charge distribution, N_{3D}, and potentials, V_σ, for a double unit cell of three different (Ga,Mn)As/(Al,Ga)As based superlattice structures in an AFM state. $d_n/\frac{1}{2}a_0=5$, $\bar{N}_{3D}=10^{20}$ cm^{-3}, and the Al concentration is 30% in each case. $V_\sigma=0$ eV corresponds to the Fermi level. (a) $d_m/\frac{1}{2}a_0=2$ and 2% Mn doping, (b) $d_m/\frac{1}{2}a_0=2$ and 8% Mn doping, and (c) $d_m/\frac{1}{2}a_0=8$ and 8% Mn doping.

there is a slight increase in the polarization of carriers over the previous two cases with 2% Mn moment, this is increased significantly when more moments (8%) are put in the magnetic layers, as shown in Fig. 2(b). Because of the strong confinement of carriers to the highly magnetic layers there is a very high polarization of carriers; this effect is enhanced over that of the 8% case with a doped GaAs spacer, which was shown in Fig. 1(b). Finally, Fig. 2(c) shows a case where the nonmagnetic layers are thinner than the magnetic layers and also have a high Mn doping. Following the established trend, carriers are strongly polarized and tightly confined to the magnetic layers. In fact, with an almost total polarization and a very high depletion of the nonmagnetic layers, this structure represents an almost opposite case to that of Fig. 1(a).

Bearing in mind these examples of how changing the structural properties can alter the electronic configuration of the superlattices, the effects of these changes on the IEC will now be explored. This will be done in two parts. First, GaAs based spacers, similar to those shown in Fig. 1 will be considered. The more extreme cases presented in Fig. 2 will be considered in the second half.

A. GaAs spacer

First to be considered is a superlattice structure close to the RKKY limit of infinitely thin magnetic layers surrounded by free unpolarized carriers. For this we shall use thin magnetic layers and a low magnetic-moment concentration, as per Fig. 1(a). In Fig. 3(a) the IEC energy, E_c, is plotted against the 3D carrier concentration, $\bar{N}_{3D}$, and the number of monolayers of GaAs in the nonmagnetic spacer, $d_n/\frac{1}{2}a_0$. The magnetic (Ga,Mn)As layer is two monolayers thick and contains 2% Mn local-moment doping. There is a uniform acceptor density throughout the structure, which gives an average hole concentration of 4.43×10^{20} cm^{-3}. In this case there are oscillations as a function of both parameters, analogous to the k_Fd oscillations in the ideal quasi-one-dimensional RKKY model. For the calculated IEC energy, E_c, positive values correspond to FM interlayer coupling being energetically favorable, and negative values correspond to AFM interlayer coupling being the favored configuration.

The RKKY-like behavior observed in Fig. 3(a) is consistent with the results obtained in the tight-binding approach[8] when the exchange coupling energy, E_c, is plotted against the two-dimensional carrier concentration, N_{2D}, for fixed layer thicknesses. However, it is worth noting that when the exchange coupling is plotted as a function of the nonmagnetic spacer thickness, d_n, for a fixed N_{2D} there are no apparent RKKY oscillations. Because N_{3D}, and therefore k_F, is a function of d_n, these two parameters are not independent when N_{2D} is fixed. This results in the oscillatory behavior appearing to be suppressed.

There are, however, real physical reasons for deviation from RKKY behavior. The data from Fig. 3(a) are replotted in Fig. 4 as a function of $2\bar{k}_Fd_{n+1}$. Also plotted is the function

$$y = \alpha\frac{\sin(x)}{x^2}, \tag{17}$$

where α is a scaling factor. This function is the asymptotic limit of the pseudo-one-dimensional RKKY range function.[17]

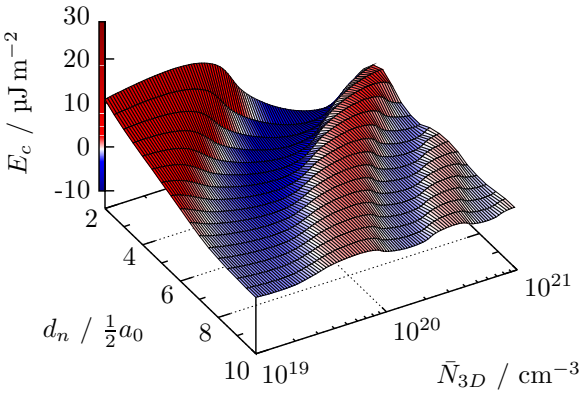

(a) $d_m/\frac{1}{2}a_0 = 2$, 2% Mn concentration

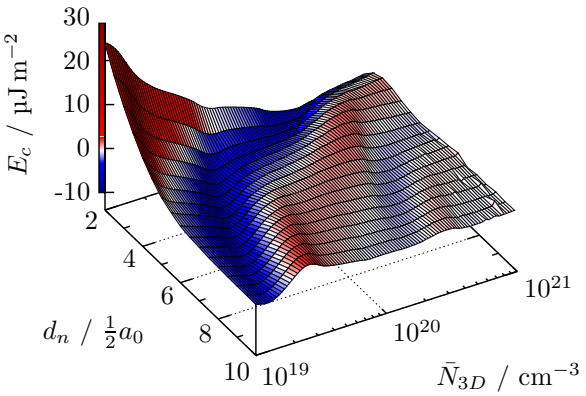

(b) $d_m/\frac{1}{2}a_0 = 8$, 2% Mn concentration

FIG. 3. (Color online) The IEC energy, E_c, of two (Ga,Mn)As/GaAs based superlattices as a function of the average 3D carrier concentration, $\bar{N}_{3D}$, and the number of monolayers of nonmagnetic layer, $d_n/\frac{1}{2}a_0$. Positive (red colored) values of E_c indicate FM interlayer coupling is energetically favorable and negative (blue colored) values indicate AFM is favorable. Both superlattices have a 2% Mn doping in the magnetic layer and there is a uniform impurity concentration of acceptors through the structure.

The strength of the interaction is expected to scale with the density of states and in the 1D case $\alpha\sim k_F^2$.[18] The different series of points on the graph correspond to the series of different nonmagnetic spacer thicknesses shown in Fig. 3(a). For a given $2\bar{k}_Fd_{n+1}$, the points with the largest magnitude are those with the greatest k_F; this behavior is consistent with the expected scaling of α with k_F. Note the fact that in order to have improved alignment of the curves the oscillations were plotted with the effective value of the nonmagnetic spacer, d_n, being increased in size by one monolayer, which is denoted d_{n+1}. This is necessary due to the fact that the magnetic layer in this structure is not infinitely thin, as per the ideal RKKY case, but has a defined width.

Exploring this deviation from RKKY behavior further, Fig. 3(b) shows the IEC for a superlattice system with a thicker magnetic layer, $d_m/\frac{1}{2}a_0=8$. All other parameters are as with (a). Examining the AFM peak, the reduction in av-

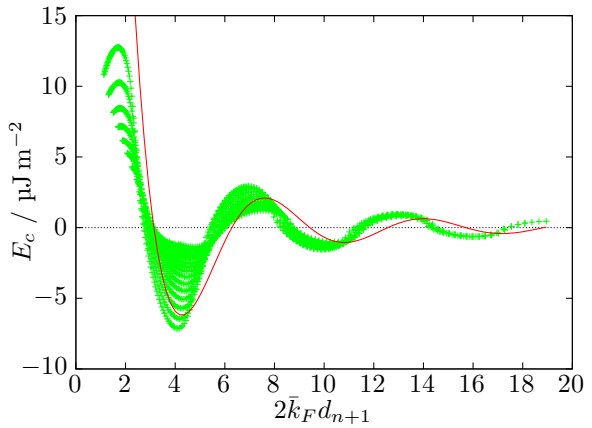

FIG. 4. (Color online) IEC energy, E_c, as a function of $2\bar{k}_F d_{n+1}$ for a superlattice with magnetic layers with a Mn doping of 2% and two monolayer thickness, and a uniform impurity concentration. The (red) curve is an estimate of the ideal RKKY range function.

erage carrier concentration of the minimum, as the spacer thickness is increased, occurs more rapidly, evidenced by the larger derivative of the average 3D carrier density, $\bar{N}_{3D}$, with respect to the nonmagnetic layer thickness, d_n, of the minimum E_c at low d_n. By way of contrast, at large d_n this is lower, that is, the curve has become much more straight. This is consistent with the effects of large magnetic layers increasing the center-to-center distance of the magnetic layers causing the effect of an apparently larger nonmagnetic layer. However, in addition to this, increasing the magnetic layer thickness has introduced additional points of inflection for reasons that are not immediately obvious.

It is also possible to deviate from RKKY-type behavior through redistribution of charge. There are two primary methods by which this is achieved, as shown in Figs. 1(b) and 1(c). The first is that charge is confined to the magnetic layers by the magnetic exchange potential. Figure 5(a) shows the IEC where the Mn doping has been increased to 8%. However, when the magnetic layer is thin, significant charge redistribution is opposed by the Coulomb potential and the RKKY character is not significantly affected. As the figure shows, the main effect is that the size of the IEC is increased. Despite the larger spin splitting and the larger polarization of carriers caused by the greater moment concentration, the coupling retains an RKKY character.

When the magnetic layer is made wider the increased quantity of magnetic moments now causes additional changes in the oscillatory behavior, beyond that of simply increasing d_m. Figure 5(b) plots the IEC for a system which now has magnetic layers of eight monolayers with a Mn doping of 8%. Because of the increased depletion of carriers from the nonmagnetic layers, the N_{3D} values at which AFM coupling is expected to occur are now greater for a given nonmagnetic layer thickness. Additionally, the damping of the magnitude of the IEC energy with increasing d_n has now significantly changed. While the first FM and AFM maxima are rapidly diminished with increasing nonmagnetic spacer, the second FM peak is not greatly affected. The second AFM peak even increases in magnitude with larger d_n, and for large spacer it can even be greater than the first.

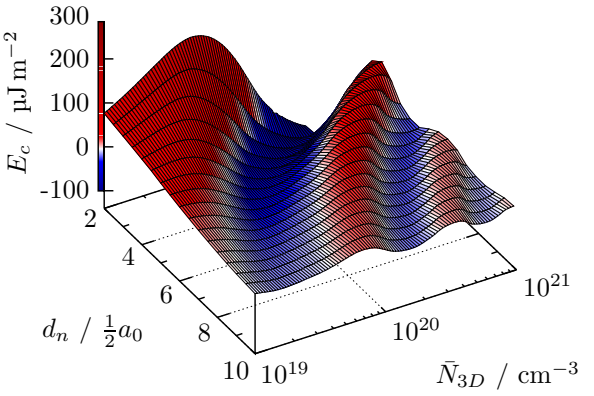

(a) $d_m/\frac{1}{2}a_0 = 2$, 8% Mn concentration

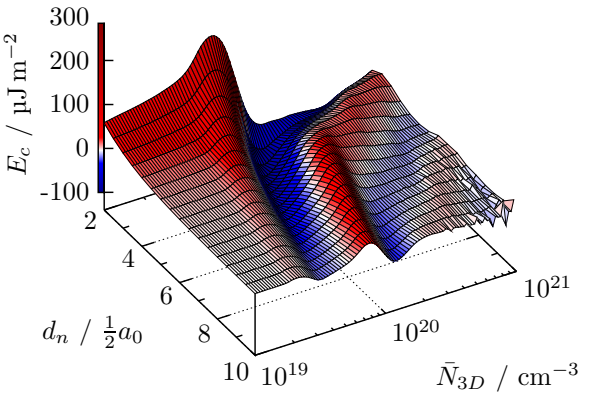

(b) $d_m/\frac{1}{2}a_0 = 8$, 8% Mn concentration

FIG. 5. (Color online) The IEC energy, E_c, of two (Ga,Mn)As/GaAs based superlattices as a function of the average 3D carrier concentration, $\bar{N}_{3D}$, and the number of monolayers of nonmagnetic layer, $d_n/\frac{1}{2}a_0$. Both superlattices have an 8% Mn doping in the magnetic layer and there is a uniform impurity concentration of acceptors through the structure.

Note that when the unit cell becomes large and there is a high carrier concentration, the weak coupling and flat minibands make self-consistent convergence difficult; these regions are visible as rough areas on the figures. Such samples would anyway be extremely sensitive to inhomogeneities and fluctuations. No data is shown where the calculations have diverged.

The second method of charge redistribution is via Coulomb potential. Figure 6(a) shows the IEC profile for a system with a magnetic spacer of two monolayers and a Mn concentration of 2%. However, now there is no neutralizing background charge in the nonmagnetic layer so self-consistent redistribution results in the formation of an effective barrier. Figure 1(c) shows the potentials and charge distribution for a unit cell of this structure in an AFM configuration, again with $d_n/\frac{1}{2}a_0=5$ and $\bar{N}_{3D}=10^{20}$ cm^{-3}. As previously noted, the Coulomb barrier formed is comparable in size to the spin splitting caused by the 2% Mn doping. This results in a similar charge redistribution as in the 8% doped case although without such strong carrier polarization.

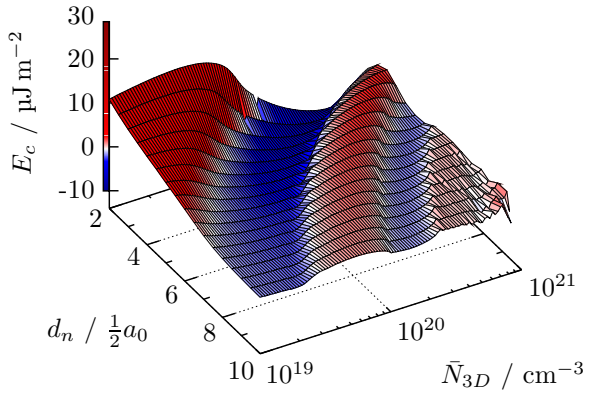

(a) $d_m/\frac{1}{2}a_0 = 2$, 2% Mn concentration

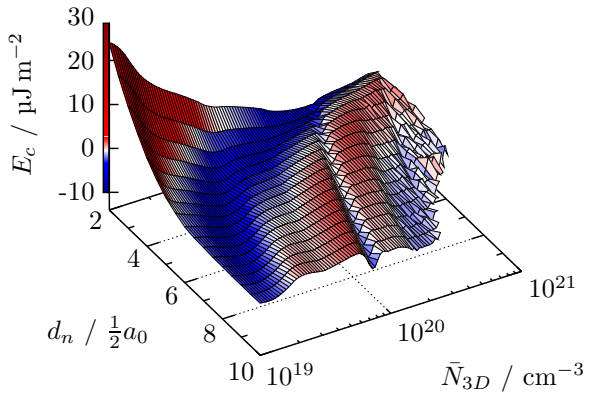

(b) $d_m/\frac{1}{2}a_0 = 8$, 2% Mn concentration

FIG. 6. (Color online) The IEC energy, E_c of two (Ga,Mn)As/GaAs based superlattices as a function of the average 3D carrier concentration, $\bar{N}_{3D}$, and the number of monolayers of nonmagnetic layer, $d_n/\frac{1}{2}a_0$. Both superlattices have a 2% Mn doping in the magnetic layer, but there is no charge doping in the nonmagnetic spacer layer.

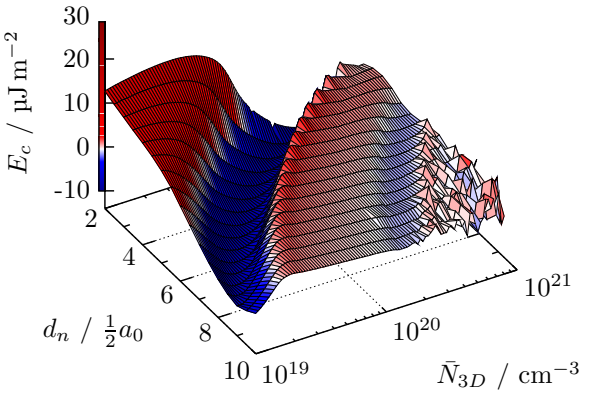

(a) $d_m/\frac{1}{2}a_0 = 2$, 2% Mn concentration

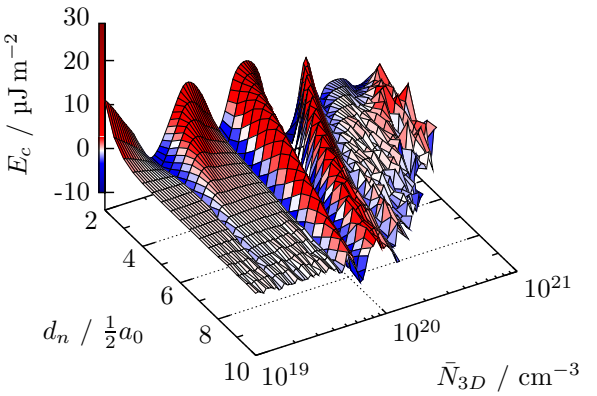

(b) $d_m/\frac{1}{2}a_0 = 8$, 2% Mn concentration

FIG. 7. (Color online) The IEC, E_c, of two (Ga,Mn)As/(Al,Ga)As based superlattices as a function of the average 3D carrier concentration, $\bar{N}_{3D}$, and the number of monolayers of nonmagnetic layer, $d_n/\frac{1}{2}a_0$. Both superlattices have a 2% Mn doping in the magnetic layer and the nonmagnetic layers are $(Al_{0.3},Ga_{0.7})As$ and have no charge doping.

As with that case, there is no significant deviation from RKKY-type behavior.

Increasing the magnetic spacer thickness now causes more significant changes than seen with the doped spacers. Figure 6(b) shows the IEC profile for a superlattice with $d_m/\frac{1}{2}a_0=8$ with a 2% Mn doping and no impurities in the nonmagnetic spacer. In addition to the extra inflection points there is now an additional AFM region. The magnitude of the local minimum in this region does not decrease much with nonmagnetic spacer width and occurs with an almost linear $d\bar{N}_{3D}/dd_n$. This is now very unlike RKKY behavior.

To investigate this further we shall now consider superlattice with (Al,Ga)As nonmagnetic spacers so that greater charge redistribution will occur than that caused by the magnetic ordering potential of a high magnetic-moment concentration or the Coulomb potential arising from an undoped spacer.

B. (Al,Ga)As spacer

In the previous section it was demonstrated that interlayer coupling in superlattice structures would have an oscillatory behavior as a function of parameters $\bar{N}_{3D}$ and d_n, analogous to that of RKKY, when the magnetic layers were thin and surrounded by charge. As the structure of the superlattice is changed the IEC would start to deviate from the ideal RKKY behavior. This is particularly apparent with increased magnetic layer thickness. Changing the 3D charge distribution has a more limited effect; neither large magnetic-moment concentration nor a self-consistent Coulomb barrier would cause significant confinement of carriers. In order to investigate these effects further, a band offset will be introduced to further confine carriers to the magnetic layers. This will be achieved by using $(Al_{0.3},Ga_{0.7})As$ as the nonmagnetic layer material, which has a valence-band offset of about 150 meV from GaAs.[19,20]

Figure 7(a) shows the IEC profile for a structure with a $(Ga_{0.98},Mn_{0.02})As$ magnetic layer of two monolayers and an

$(Al_{0.3},Ga_{0.7})As$ nonmagnetic layer. There is no doping in the nonmagnetic layers. The peak FM and AFM coupling strengths are now stronger than in the case with doped GaAs spacers seen in the otherwise identical structure in Fig. 3(a). The charge distribution of this structure is shown in Fig. 2(a) where the barrier confines carriers to the magnetic layers as expected. However, the $2d_n\bar{k}_F$ oscillations are damped more rapidly than with the GaAs spacer, resulting in the second FM and AFM peaks being very weak. This additional damping occurs particularly rapidly with increasing carrier density, $\bar{N}_{3D}$. As a result, the first antiferromagnetic peak barely reduces in magnitude as the nonmagnetic layer thickness is increased. Juxtaposing this with the GaAs barrier case, where the largest AFM coupling that can occur when $d_n/\frac{1}{2}a_0=10$ is less than a quarter of the size of that when $d_n/\frac{1}{2}a_0=2$, we identify this as a significant departure from the previously seen RKKY-like oscillatory behavior.

Increasing the magnetic-moment concentration leads to a more interesting alteration than with the GaAs spacer where the effect was principally to scale up the magnitude of the IEC energy. Figure 8(a) shows the IEC for a (Ga,Mn)As/(Al,Ga)As superlattice with an 8% Mn doping in the two monolayer magnetic layers, as previously considered in Fig. 2(b). Now the first AFM peak appears to have two stages. The first is at low spacer thicknesses where the average hole density at which the maximum occurs decreases with increasing spacer thickness. For large spacer thicknesses the curve has straightened out and there is almost no dependence on d_n for the sign of the coupling. This characteristic is similar to that exhibited in Figs. 3(b) and 5(b), where the magnetic layer is eight monolayers thick. This was attributed to loss of independence of the d_n and $\bar{N}_{3D}$ parameters as the system became less RKKY-like. Knowing that the band offset and large magnetic ordering cause significant carrier redistribution, particularly, this means that the carrier concentration in the spacer will decrease as a function of spacer thickness. This can account for the weak dependence of E_c on k_Fd_n. Also, note that the size of the first AFM peak decreases more rapidly at high spacer thicknesses where the average carrier concentration, $\bar{N}_{3D}$, at which it occurs is not decreasing. This is consistent with the previous observation of enhanced damping with increasing carrier concentration.

With high magnetic layer thicknesses the RKKY-type oscillations have almost completely disappeared. The beating patterns which were emerging in the $d_m/\frac{1}{2}a_0=8$ GaAs spacer cases have now come to dominate the IEC. Figures 7(b) and 8(b) shows this for $d_m/\frac{1}{2}a_0=8$, with, respectively, 2% and 8% Mn doping. In these cases the oscillations occur almost exclusively as a function of hole density, being almost independent of the spacer thickness. Note, however, as was seen in Fig. 2(c), the nonmagnetic layer is highly depleted when the magnetic layer is eight monolayers thick with an 8% Mn doping. This makes computing IEC for larger spacers unfeasible.

IV. DISCUSSION AND RECIPES

Having explored the parameter spaces we will now consider possible structures of a (Ga,Mn)As based superlattice

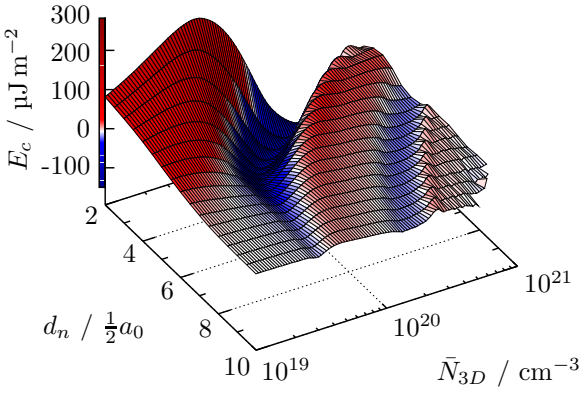

(a) $d_m/\frac{1}{2}a_0 = 2$, 8% Mn concentration

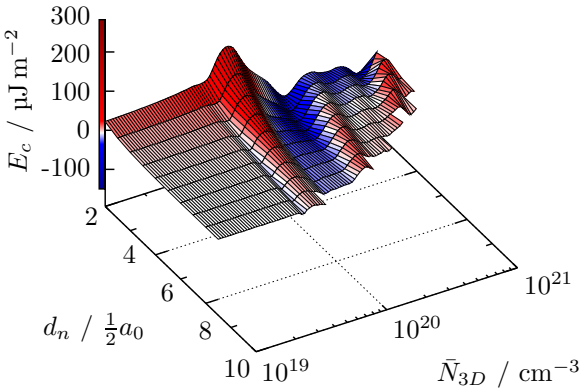

(b) $d_m/\frac{1}{2}a_0 = 8$, 8% Mn concentration

FIG. 8. (Color online) The IEC, E_c, of two (Ga,Mn)As/(Al,Ga)As based superlattices as a function of the average 3D carrier concentration, $\bar{N}_{3D}$, and the number of monolayers of nonmagnetic layer, $d_n/\frac{1}{2}a_0$. Both superlattices have an 8% Mn doping in the magnetic layer and the nonmagnetic layers are $(Al_{0.3},Ga_{0.7})As$ and have no charge doping.

that would exhibit AFM interlayer coupling. Each parameter will be considered for feasibility, and based on the above calculations, suggestions for values can be made.

The first to be considered is the Mn concentration in the (Ga,Mn)As layers. From the viewpoint of simply creating a viable ferromagnet this is an essential parameter; not only does each substitutional Mn provide a magnetic moment, it also acts as an acceptor and thus this factor controls the hole concentration. Calculations[21] estimate that the minimum hole density for ferromagnetism is $\sim 10^{20}$ cm^{-3}. Assuming that each Mn provides one hole, this carrier concentration would correspond to a moment concentration of ~0.5%. Experimentally, typical Mn concentrations are in the range of 2%–8% (4.4×10^{20}–1.8×10^{21} cm^{-3}), which in good quality material could result in higher carrier concentrations than the 10^{19}–10^{21} cm^{-3} range considered in these calculations. While the higher magnetic-moment concentration can increase the size of the E_c peak, and thus a high moment concentration is favorable; the high carrier concentrations that would be associated with this would cause the strength of the

IEC to become extremely weak. This constraint therefore imposes a practical range for Mn concentrations as being between 2% and 4% (4.4×10^{20}–8.8×10^{20} cm^{-3}, respectively).

For the nonmagnetic spacer thickness the general trend is that the strength of the IEC becomes weaker as the nonmagnetic layer becomes thicker. Although this effect is somewhat diminished for the cases where there is strong carrier confinement to the magnetic layers, it is a serious consideration and, ideally, to see strong IEC effects, the nonmagnetic layer should be as thin as possible. Furthermore, particularly in cases where the $2k_Fd$ behavior is dominant, as carrier concentration increases the spacer thickness at which the AFM IEC is strongest decreases inversely. As discussed above, low carrier concentrations are not possible; so therefore it would seem beneficial to make the spacer layers as thin as practicable. Bearing in mind that the average distance between two Mn atoms when the concentration is 3% is of the order of a couple of GaAs unit cells, in order to make the nonmagnetic spacer a discernible barrier then four monolayers would seem to be a realistic lower bound.

The effect of the magnetic layer thickness on the IEC profile is more subtle and seems mainly to distort the RKKY behavior but otherwise, in the limits considered within this study, does not have any negative effects on the interlayer coupling. However, again for interlayer coupling to exist it is necessary that each magnetic layer is itself ferromagnetic. Usually (Ga,Mn)As is grown in bulk layers of many nanometers; the thinnest (Ga,Mn)As epilayers for which published literature exists are 5 nm thick,[22] and the (Ga,Mn)As based heterostructures with magnetic layers as thin as eight monolayers have been reported to be ferromagnetic.[23] It would therefore seem prudent, in order to ensure that the magnetic layers are effective ferromagnets, to prefer to make them thicker. For the 5 nm film some amount of surface depletion should be expected, so an eight monolayer thick magnetic layer, equivalent to 2.26 nm, is comparable. Of course, if thinner films are shown to be viable then there is no reason not to consider them also.

Based on these constraints, Fig. 9 shows the IEC profile for two candidate superlattices as a function of carrier concentration, $\bar{N}_{3D}$. Both superlattices are identical in structure except for the composition of the nonmagnetic layer. The magnetic layer thickness is eight monolayers and has a magnetic impurity concentration of 5×10^{20} cm^{-3} (2.26%), and the nonmagnetic layers are four monolayers thick. As expected from the calculations, when the (Al,Ga)As barriers strongly confine carriers to the magnetic layers the IEC energy can have potentially greater magnitudes although the oscillations have a much higher frequency. In these samples the carrier concentration would be somewhere below the Mn concentration of 5×10^{20} cm^{-3} (2.26%); however the exact amount would depend on subtleties of the growth conditions. Although this suggests that for AFM IEC to occur the desired carrier concentration should be several times lower, it must be accepted that the calculations are of a more qualitative nature. Additionally, by tailoring the band offset of the nonmagnetic layer by altering the Al content, the location of the peak can be somewhat adjusted. This at least shows that these designs offer the possibility for AFM interlayer coupling.

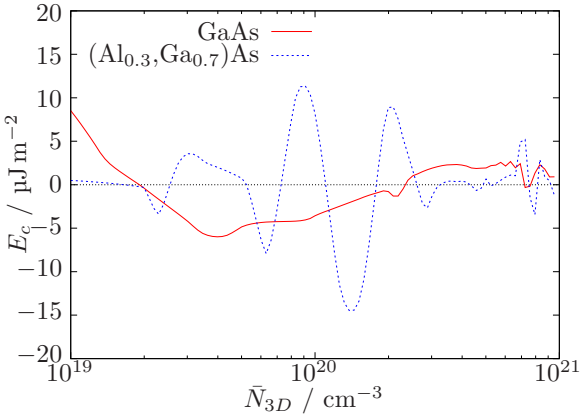

FIG. 9. (Color online) A comparison of the IEC energy, E_c, as a function of the average 3D carrier concentration, $\bar{N}_{3D}$, for two specific superlattices with either a GaAs or an $(Al_{0.3},Ga_{0.7})As$ nonmagnetic layer. The magnetic layers are eight monolayers thick and have a Mn concentration of 5×10^{20} cm^{-3} (2.26%) and the nonmagnetic layers are four monolayers thick.

Even if the IEC energy were to favor an AFM arrangement, if the AFM coupling is weaker than the anisotropy fields it is possible that after the application of a field the superlattice could become locked into a FM spin configuration. This spin-locking behavior has been observed in EuS/PbS superlattices[6] and Fe/Nb multilayers[24] studied via neutron scattering.

Comparing, then, the calculated IEC to the magnetocrystalline anisotropic energy of (Ga,Mn)As, we take a typical "worst case" value of the in-plane cubic anisotropy constant to be of the order of 2000 J m^{-3} at 4.2 K.[25] Using a value of the interlayer coupling energy $E_c=10$ μJ m^{-2} from Fig. 9 and using the bilayer period of 3.4 nm, we find that the energy density of the IEC energy is 3000 J m^{-3}. Although this is assuming an ideal value of E_c, this compares favorably with the anisotropy energy. Furthermore, larger values for the IEC have been found in the tight-binding approach.[8] Therefore, such a superlattice structure might reasonably be expected to be a candidate to exhibit AFM interlayer coupling.

V. CONCLUSION

The composition and structure of (Ga,Mn)As based superlattices can have profound effects on the expected IEC. By examining possible compositions within the broad parameter space that these structures offer it is possible to identify different recipes for devices that might offer the possibility of demonstrating AFM interlayer coupling. Such a study was presented in this paper based on the parabolic band $\mathbf{k}\cdot\mathbf{p}$ kinetic-exchange model. This model ignores spin-orbit and band warping effects although comparisons to the previously studied microscopic tight-binding model suggest that our results provide a reasonable qualitative or semiquantitative description of the system. The calculations predict that short period superlattices with magnetic and nonmagnetic layers with widths less than ten monolayers seem to be promising candidates. There is existing experimental work in

(Ga,Mn)As/GaAs based superlattices with similar dimensions, but this has only exhibited FM IEC.[23,26] The ideal dimensions suggested by the calculations are therefore feasible and have shown themselves to be viable ferromagnetic DMS material.

Particularly interesting, in a (Ga,Mn)As/(In,Ga)As based superlattice composed of four and eight monolayer width layers, respectively, two phase transitions were observed.[27] Although there was no evidence that this was due to any AFM effects, this indicates that there is some additional physics at play in these systems making them of interest for further study. The calculations presented in this paper have shown the importance of the composition of the nonmagnetic spacer on the character of the IEC. Using different Al concentrations to tailor the band offset between layers in a superlattice is a standard tool for designing normal nonmagnetic superlattice systems. Utilizing this technique in the magnetic superlattices could potentially provide a way to tune to IEC profile to one where AFM coupling is preferential.

ACKNOWLEDGMENTS

We acknowledge support from EU Grant No. IST-015728, from UK Grant No. GR/S81407/01, and from CR Grants No. KAN400100652, No. FON/06/E002, No. AV0Z1010052, and No. LC510.

[1] M. N. Baibich, J. M. Broto, A. Fert, F. Nguyen Van Dau, F. Petroff, P. Eitenne, G. Creuzet, A. Friederich, and J. Chazelas, Phys. Rev. Lett. **61**, 2472 (1988).
[2] E. Vélu, C. Dupas, D. Renard, J. P. Renard, and J. Seiden, Phys. Rev. B **37**, 668 (1988).
[3] G. Binasch, P. Grünberg, F. Saurenbach, and W. Zinn, Phys. Rev. B **39**, 4828 (1989).
[4] P. Bruno, Phys. Rev. B **52**, 411 (1995).
[5] V. Nunez, T. Giebultowicz, W. Faschinger, G. Bauer, H. Sitter, and J. Furdyna, J. Magn. Magn. Mater. **140-144**, 633 (1995).
[6] H. Kępa, J. Kutner-Pielaszek, J. Blinowski, A. Twardowski, C. F. Majkrzak, T. Story, P. Kacman, R. R. Gałazka, K. Ha, H. J. M. Swagten, W. J. M. de Jonge, A. Yu. Sipatov, V. Volobuev, and T. M. Giebultowicz, Europhys. Lett. **56**, 54 (2001).
[7] T. Jungwirth, W. A. Atkinson, B. H. Lee, and A. H. MacDonald, Phys. Rev. B **59**, 9818 (1999).
[8] P. Sankowski and P. Kacman, Phys. Rev. B **71**, 201303(R) (2005).
[9] D. Chiba, N. Akiba, F. Matsukura, Y. Ohno, and H. Ohno, Appl. Phys. Lett. **77**, 1873 (2000).
[10] H. Kępa, J. Kutner-Pielaszek, A. Twardowski, C. F. Majkrzak, J. Sadowski, T. Story, and T. M. Giebultowicz, Phys. Rev. B **64**, 121302(R) (2001).
[11] S. J. Chung, S. Lee, I. W. Park, X. Liu, and J. K. Furdyna, J. Appl. Phys. **95**, 7402 (2004).
[12] C. Zener, Phys. Rev. **81**, 440 (1951).
[13] T. Jungwirth, J. Sinova, J. Mašek, J. Kučera, and A. H. MacDonald, Rev. Mod. Phys. **78**, 809 (2006).
[14] C. Kittel, in *Solid State Physics: Advances in Research Applications*, edited by F. Seitz, D. Turnbull, and H. Ehrenreich (Academic, New York, 1968), Vol. 22, pp. 1–26.
[15] J. Sinova, T. Jungwirth, and J. Černe, Int. J. Mod. Phys. B **18**, 1083 (2004).
[16] S. H. Vosko, L. Wilk, and M. Nusair, Can. J. Phys. **58**, 1200 (1980).
[17] Y. Yafet, Phys. Rev. B **36**, 3948 (1987).
[18] T. Dietl, A. Haury, and Y. M. d'Aubigné, Phys. Rev. B **55**, R3347 (1997).
[19] J. Batey and S. L. Wright, J. Appl. Phys. **59**, 200 (1986).
[20] I. Vurgaftman, J. R. Meyer, and L. R. Ram-Mohan, J. Appl. Phys. **89**, 5815 (2001).
[21] T. Jungwirth, K. Y. Wang, J. Mašek, K. W. Edmonds, J. König, J. Sinova, M. Polini, N. A. Goncharuk, A. H. MacDonald, M. Sawicki, A. W. Rushforth, R. P. Campion, L. X. Zhao, C. T. Foxon, and B. L. Gallagher, Phys. Rev. B **72**, 165204 (2005).
[22] A. D. Giddings, M. N. Khalid, T. Jungwirth, J. Wunderlich, S. Yasin, R. P. Campion, K. W. Edmonds, J. Sinova, K. Ito, K.-Y. Wang, D. Williams, B. L. Gallagher, and C. T. Foxon, Phys. Rev. Lett. **94**, 127202 (2005).
[23] J. Sadowski, R. Mathieu, P. Svedlindh, M. Karlsteen, J. Kanski, Y. Fu, J. T. Domagala, W. Szuszkiewicz, B. Hennion, D. K. Maude, R. Airey, and G. Hill, Thin Solid Films **412**, 122 (2002).
[24] C. Rehm, D. Nagengast, F. Klose, H. Maletta, and A. Weidinger, Europhys. Lett. **38**, 61 (1997).
[25] K.-Y. Wang, M. Sawicki, K. W. Edmonds, R. P. Campion, S. Maat, C. T. Foxon, B. L. Gallagher, and T. Dietl, Phys. Rev. Lett. **95**, 217204 (2005).
[26] W. Szuszkiewicz, E. Dynowska, B. Hennion, F. Ott, M. Jouanne, and J. F. Morhange, Acta Phys. Pol. A **100**, 335 (1998).
[27] C. Hernandez, F. Terki, S. Charar, J. Sadowski, D. Maude, V. Stanciu, and P. Svedlindh, Acta Phys. Pol. A **103**, 613 (2001).